

This is the **submitted version** of the journal article:

Saiz-Poseu, Javier; Sedó Vegara, Josep; Garcia, Beatriz; [et al.]. «Versatile nanostructured materials via direct reaction of functionalized catechols». *Advanced materials*, Vol. 25, issue 14 (April 2013), p. 2066-2070. DOI 10.1002/adma.201204383

This version is available at <https://ddd.uab.cat/record/279303>

under the terms of the  ^{IN} COPYRIGHT license

Versatile Functional Materials via Direct Polymerization of Catechols

By *Javier Saiz-Poseu, Josep Sedó, Beatriz García, Cristina Beneiges, Ramon Alibés, Jordi Hernando, Felix Busqué* and Daniel Ruiz-Molina**

[*] Dr. D. Ruiz-Molina, Dr. J. Sedó.

Centro de Investigación en Nanociencia y Nanotecnología (CIN2, CSIC), Esfera UAB
Edificio CM7, Campus UAB, 08193 Cerdanyola del Vallés (Spain)

E-mail: druiz@cin2.es

C. Beneiges, Dr. F. Busqué, Dr. J. Hernando, Prof. R. Alibés
Department de Química, Universitat Autònoma de Barcelona,
Edifici C, Campus UAB, 08193
Cerdanyola del Vallès (Spain)

Dr. J. Saiz-Poseu, B. García

Fundación Privada ASCAMM, Unidad de Nanotecnología (NANOMM) Parc Tecnològic del
Vallès, Av. Universitat Autònoma, 23 - 08290
Cerdanyola del Vallès (Spain)

Keywords: catechol, adhesive properties, coatings, oleo-/hydrophobic-hydrophilic, nanoparticles

Mussel-adhesive proteins have been the subject of intensive scientific research over the past decades,^[1,2,3,4] associated to the remarkable ability of marine invertebrates to strongly adhere to virtually all surfaces, even low-fouling materials.^[3,5] Albeit diverse in structure, this behavior has been attributed to their varying amounts of the non-essential catecholic aminoacid DOPA.^[1,5] Since this discovery, an ever-increasing number of bioinspired catechol-based polymers have been reported,^[6] and shown to constitute powerful tools for the fabrication of water-resistant adhesives,^[7] protective layers,^[8] primers for functional adlayers and nanoscale coatings,^[9] among others.^[10] In all these cases, functional catechol-based materials were obtained by incorporation of catecholic moieties into more or less complex functional polymers. Messersmith and co-workers^[11] reported an easy and straightforward method for the preparation of polydopamine by oxidative polymerization of the dopamine catechol.^[12] The process allows for the *in situ* deposition of -otherwise highly insoluble- polymeric material on a wide variety of substrates,^[13] which can be further functionalized on a

second step in a versatile way though with an uncontrolled functionalization degree. Other research groups have reported on the preparation of macromolecular systems bearing “adhesive” catecholic moieties, plus one or more functional chains grafted to a common polymeric backbone.^[8c-e] These design strategies afford control of the polymer structure and degree of functionalization, and the possibility of deposition by means of *ex situ* treatments, but otherwise involve the use of careful polymerization procedures to circumvent undesired or premature catechol reactivity.

Here we report an alternative and simple polymerization method consisting in the direct reaction of functional catechols with an excess of aqueous ammonia. In addition to maintaining a mildly basic pH necessary for the fast oxidation of the catechol ring under aerobic conditions, ammonia may act as a nucleophile on the reactive *o*-quinones thus formed, in a way reminiscent of melanization reactions such as that used in the preparation of polydopamine. In this sense, ammonia might provide the desired covalent cross-link between adjacent catechol rings, independently of their substitution pattern. As a first proof of concept, we chose amphiphile 4-heptadecylcatechol **1**. In addition to be shown to exhibit a considerable tendency to adhere to surfaces,^[14] compound **1** is closely related to alkylcatechols found in urushiol,^[15] used for thousands of years on protective lacquered coatings. The resulting polymerization product is amenable to deposition on representative nanostructures, as well as flat and convoluted bulk surfaces of very different chemical nature, by simple and fast *ex situ* procedures on organic solvents. As befitting the structure of monomer **1**, these coatings were shown to confer a robust hydrophobic character to the surfaces. Moreover, thanks to the amphiphilic character of **1**, the new material could be itself structured and isolated in the form of nanoparticles exhibiting excellent adhesion to textile materials.

In a typical experiment, a large excess of aqueous ammonia (100:1) was slowly added under vigorous stirring in the presence of air to a solution of **1** (0.2 % , w/v) in methanol, at 40 °C.

The transparent, colorless solution turned bright orange, and later to a turbid dark-brown dispersion after several hours, which was attributed to the onset and further progress of the oxidative polymerization. Thin-layer chromatography (TLC) was used to follow the reaction, showing that approximately 80% of monomer **1** had already reacted after 3 hours, and consumed quantitatively within 24 hours, after which a dark-brown amorphous solid (**2**) could be extracted with chloroform and isolated by evaporation. Lower ammonia excesses (2, 5 and 10:1) caused the reaction to advance extremely slowly, while a molar excess of 1000:1 did not result in significant modifications neither of the material nor the reaction time. A complete characterization of compound **2** obtained upon filtration and drying was attempted by NMR, EPR, FT-IR, mass-spectrometry, elementary analysis and XPS (see supplementary material). From there, little detailed information on the structure of the polymeric material can be obtained, but the incorporation of nitrogen, based on elementary analysis results and XPS, and the presence of the long alkyl chains, according to NMR data, were confirmed. MS results pointed out to a low polymerization degree of no more than 6-7 average units. Taking into account the many possible variations in the reaction pathway that may be occurring simultaneously (Michael-type additions, Schiff-base formation, direct radical aryl-aryl couplings, a.o.), the difficulty in the elucidation of the structure of **2** is not surprising, and seems otherwise closely reminiscent with those encountered in the study of natural and synthetic melanins,^[16] and polydopamine^[17] itself.

Interestingly, the morphological characterization by SEM and TEM of polymer **2** as *directly* obtained from the (polar) reaction medium upon evaporation of the ammonia excess, revealed its structuration into solid nanoparticles (NPs) with diameters ranging from 100 to 350 nm (see **Fig. 1a-b**). The surface charge of the NP suspension (measured as zeta potential) was found to be around -45 mV in water at pH \approx 7, which would be in agreement with the presence of a certain amount of catechol groups in the outermost layer, providing a proper stability of the colloidal suspension for many days. **2**-NPs also exhibit fluorescence emission

spanning over the whole visible spectral region, as shown in **Fig. 1c**. This indicates that conjugated polymeric segments are formed by polymerization, since the absorption spectrum of **1** lies within the UV region. On the other hand, the extremely broad fluorescence spectrum measured for **2**-NPs further confirms that they must be constituted by a polydisperse mixture of oligomers/polymers of **1**, which should present different conjugation lengths depending on the polymerization degree and, therefore, distinct absorption and emission spectra within the UV-vis region.

Finally, as expected from the presence of exposed catecholate groups in the outermost layer, the adhesiveness of **2**-NPs was tested on polyester fibers. This was done simply by dipping a piece of polyester in a water suspension of **2**-NPs, without any specific pre-treatment or functionalization. SEM images of the treated polyester fabric (**Fig. 1d-e**) showed that a large number of nanoparticles are adhered around individual fibers nicely distributed over the whole sample, even after drying under a vigorous nitrogen flow. This result is relevant in view of the challenge posed by the functionalization of textile fabrics with organic nanoparticles.^[18]

-Insert Figure 1 here-

When compound **2** is dissolved in non polar solvents, such as chloroform or hexane, SEM images reveal the conversion of the NPs into an amorphous material that is subsequently used to coat nanoscopic materials by the simple and quick dipping method schematically depicted in **Fig. 2a**. As a proof-of concept, iron oxide nanoparticles of 500-650 nm in diameter were dispersed in a 0.5% (w/v) *n*-hexane solution of **2** for 30 minutes and filtered. TEM images showed that treated NPs appear surrounded by a brighter halo (not apparent in the non-treated sample) that corresponds to the presence of a 5 to 50 nm thin film of **2**, (see supplementary material).^[19] Similar results were obtained for 250-600 nm mesoporous silica NPs, affording

coating thicknesses ranging from 7 to 20 nm (see supplementary material). Finally, MWCNTs were also coated upon dispersion by ultrasonication in a methanol solution of **2**. As can be seen in **Fig. 2b**, the coating can be differentiated as an outer layer with brighter contrast (orange arrows), around the darker nanotube walls (green arrows). Different concentrations (0.1, 1 and 5% w/v) and dipping times (5 and 60 minutes) led to very similar results with very homogeneous coating layers around the MWCNTs, ranging in all the cases from 4 to 7 nm.^[20] The coating modifies the surface characteristics of the MWCNTs conferring a more hydrophobic character (**Fig. 2c**), so MWCNTs tend to float on a water solution without settling, even after vigorous ultrasonication and stirring, as opposed to uncoated nanotubes, which disperse temporally upon sonication. In contrast, long standing -though not perfectly homogeneous- suspensions of treated MWCNTs are obtained in a less polar solvent such as ethyl acetate, where uncoated MWCNTs exhibit a more pronounced tendency to aggregate.

-Insert Figure 2 here-

The coating capacity of **2** was also confirmed and evaluated on a glass slide, following the same procedure described in Fig 2a and using a 1% (w/v) *n*-hexane solution of **2** for 1 minute. The corresponding AFM image shown in **Fig. 3b** reveals a very homogeneous coating with a surface roughness inferior to 0.2 nm, and an average thickness of approximately 150 nm, as determined by measuring the topographic profile of a scratched zone (see supplementary material). In optimized coating conditions, treated glasses exhibit reproducible contact angles (CA) around 100°, considerably higher than those of the untreated glass (15-20°) and well in the hydrophobic limit expected for smooth surfaces.^[21] These values were found to be insensitive to longer dipping times, revealing no significant differences between treatments lasting up to 24 hours. On the contrary, CAs were found to depend on parameters such as solvent nature or concentration (see supplementary material). These results are comparable

with those already described for polydopamine-derived coatings already used for the modification of surface energies.^[22]

In order to test resistance of the outside layer, coated glass substrates were subsequently subject to thermal treatment by heating in an oven at 90 °C, and washing stress tests (with water and methanol). In both cases, CA remain approximately unchanged, with slight variations that lay within experimental error. This behavior is in contrast with that of the hydrophobic coating obtained upon self-assembly of a monolayer of unreacted compound **1** on glass, which exhibits smaller CA values and especially, much lower thermal and wear resistance (see supplementary material). Both facts confirm the need for the polymerization of **1** into the cross-linked product **2** to ensure a robust and feasible coating.

The hydrophobic character was also investigated on 2 x 2 cm² polyester samples treated with a 1% w/v *n*-hexane solution of **2** for 1 minute. SEM images of the coated textiles are shown in **Fig. 3a**. Differences in fabric thickness between treated and non-treated substrates are not discernible in SEM images at first sight, unless a small area lacking proper coating is magnified. More evident is the coating when using concentrations as high as 10% (see supplementary material), though in all cases fibers still show ample room between each other, which is relevant to ensure that the mechanical properties and breathability of the uncoated textiles are preserved upon deposition of **2**. In accordance with the hydrophobic nature of monomer **1** and the intrinsic roughness of the textile substrate, a high CA value of 130° is obtained, which is maintained indefinitely, in contrast with the quick absorption of water on the pristine textile. No significant improvement of the CA can be detected across the whole concentration range of **2** used.

In order to expand the scope of modification of surface energies -from oleophobic to hydrophilic- by means of ammonia-reacted polymers of functional catechols, the same polymerization reaction was tried on a related catechol bearing a partially fluorinated alkyl chain (**3**), and on simple pyrocatechol (**4**). In both cases, the reaction worked in a similar

fashion, and functional coatings were obtained in accordance with the nature of the respective monomers. For instance, treatment of a glass slide and a piece of polyester textile with the polymerization product of **3** in a 0.5 % (w/v) solution in THF afforded CAs of 115° and 150°, respectively. Thus, and thanks to its fluorinated character, treated surfaces exhibited not only hydrophobic, but also oleophobic character (see **Fig. 3c** and video on supplementary material). On the other hand, treatment with an aqueous solution of the polymerization product of **4** confers a strong hydrophilic character to surfaces, as exemplified by a hydrophobic aluminum substrate, the CA of which dropped dramatically from its original 80° to 0° upon coating.

-Insert Figure 3 here-

In summary, we report a new methodology for the fabrication of catechol-based materials derived from the polymerization of functionalized catechols with ammonia. Overall, the strategy reported combines advantages such as ease of preparation, solubility in appropriate solvents, improved surface functionalization and *a priori*, a good overall density of functional moieties because each catechol ring may be designed to support a given functional chain. The as-synthesized material **2** obtained upon reaction of **1** with this new methodology, represents a nice example of the versatility of this approach. Compound **2** is shown to spontaneously structure in the form of nanoparticles a few hundred nanometers in diameter in water, which easily stick to polyester fibers affording stable NP coatings. Even though polydopamine nanoparticles resembling eumelanin particles that constitute *Sepia* ink have already been described in the literature,^[23] to our knowledge this is the first example where catecholic NPs have been reported to exhibit adhesive properties. On the other side, when the material is dissolved in non-polar solvents such as hexane, robust coatings on a representative variety of substrates, both at the nano-/macroscale are obtained, by means of a quick and *ex-situ* approach without any pretreatment or modification. In addition to the adhesiveness, the

presence of a long alkyl chain afforded robust functional coatings with a persistent hydrophobic character, which can be modulated upon modification of the surface tension by using other ammonia-reacted polymers of functional catechols. These results open new venues in the realization of biomimetic catechol materials.

Experimental Section

Experimental materials and methods, the synthesis and characterization of partially fluorinated catechol **3**, along with as well as additional results can be found in the Supporting Information

Supporting Information

Supporting Information is available from the Wiley Online Library or from the author

Acknowledgements

This work was supported by MICINN through projects MAT2009-13977-C03, CTQ2010-15380 and CTQ2009-07469. Generalitat de Catalunya is also grateful for project 2010VALOR00039.

Received: ((will be filled in by the editorial staff))
Revised: ((will be filled in by the editorial staff))
Published online: ((will be filled in by the editorial staff))

Figure captions

Fig. 1. (a) TEM and (b) SEM images of **2**-NPs. (c) Fluorescence emission spectrum of **2**-NPs in aqueous suspension ($\lambda_{\text{exc}}=355$ nm, $\lambda_{\text{det}}>400$ nm) and (inset) fluorescence microscopy image of **2**-NPs deposited onto glass ($\lambda_{\text{exc}}=540\text{-}552$ nm). (d) SEM image of a polyester fiber treated with a dispersion of **2**-NPs, where large amounts of these nanoparticles can be observed adhered to the fiber even after the drying process and (e) detail of one of such fibers with the attached NPs.

Fig. 2. (a) Schematic representation of the process carried out for coating the substrates with compound **2**. (b) TEM images of MWCNT coated with compound **2** after being dispersed in a 0.5% (w/v) *n*-hexane solution for 30 minutes. The green arrows mark the MWCNT wall; the orange arrows point at the coating thickness. (c) Different behavior of blank and treated MWCNT dispersed in water and ethyl acetate.

Fig. 3. (a) SEM image of a treated polyester fiber and the corresponding magnification from where the coating can be clearly differentiated. (b) AFM Topography image of a glass substrate ($5\mu\text{m} \times 5\mu\text{m}$) treated *ex situ* with a 1% (w/v) *n*-hexane solution of **1** for 1 minute. (c) Contact angles obtained with different liquid on different substrates coated with the polymerization product of **3**.

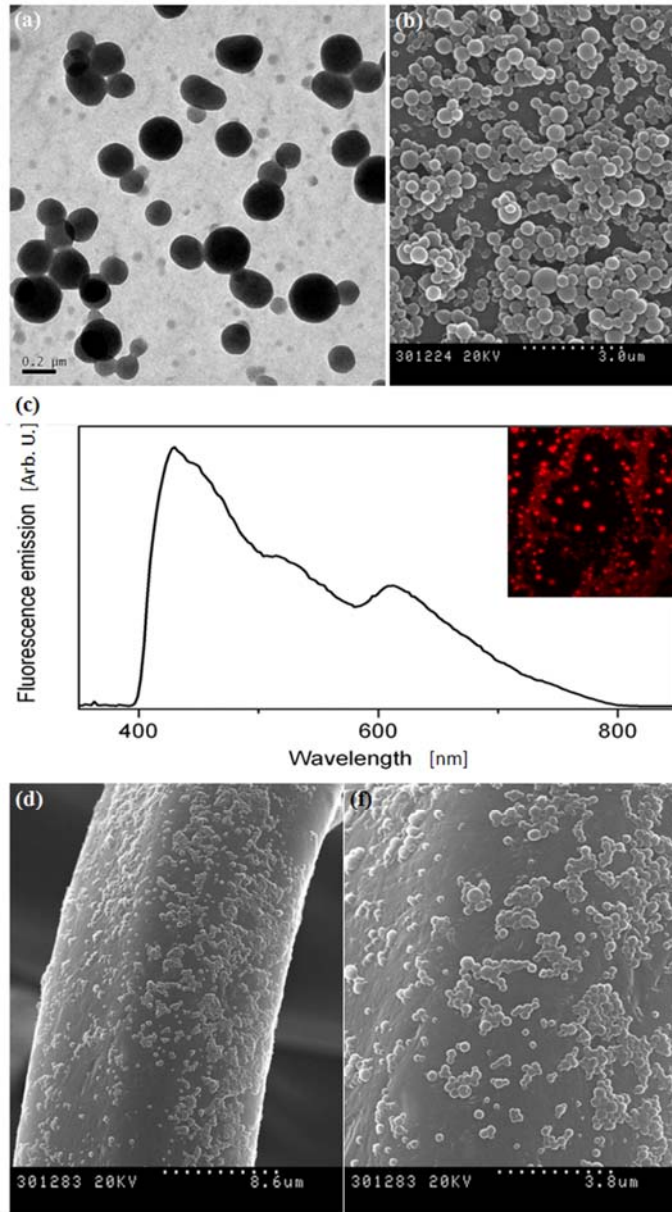


Figure 1

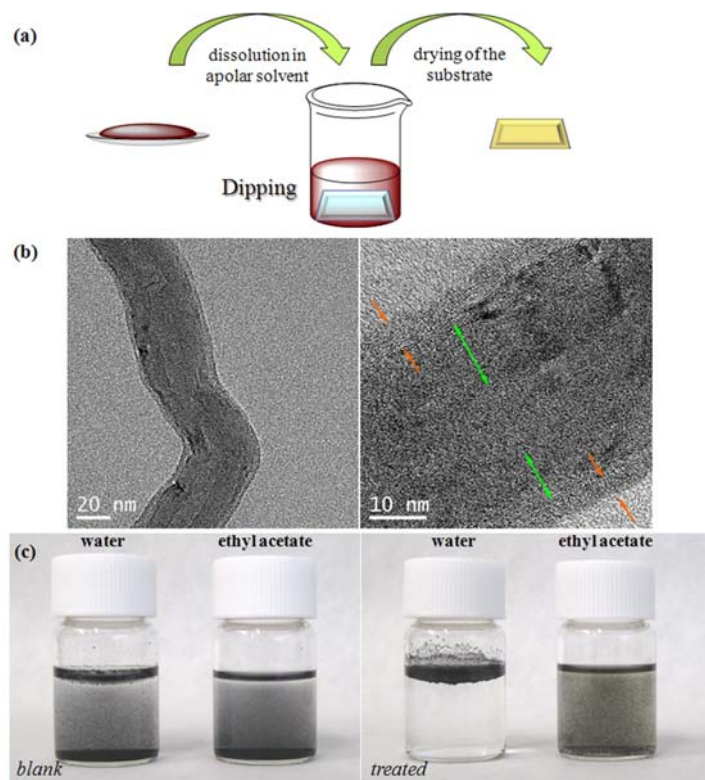


Figure 2

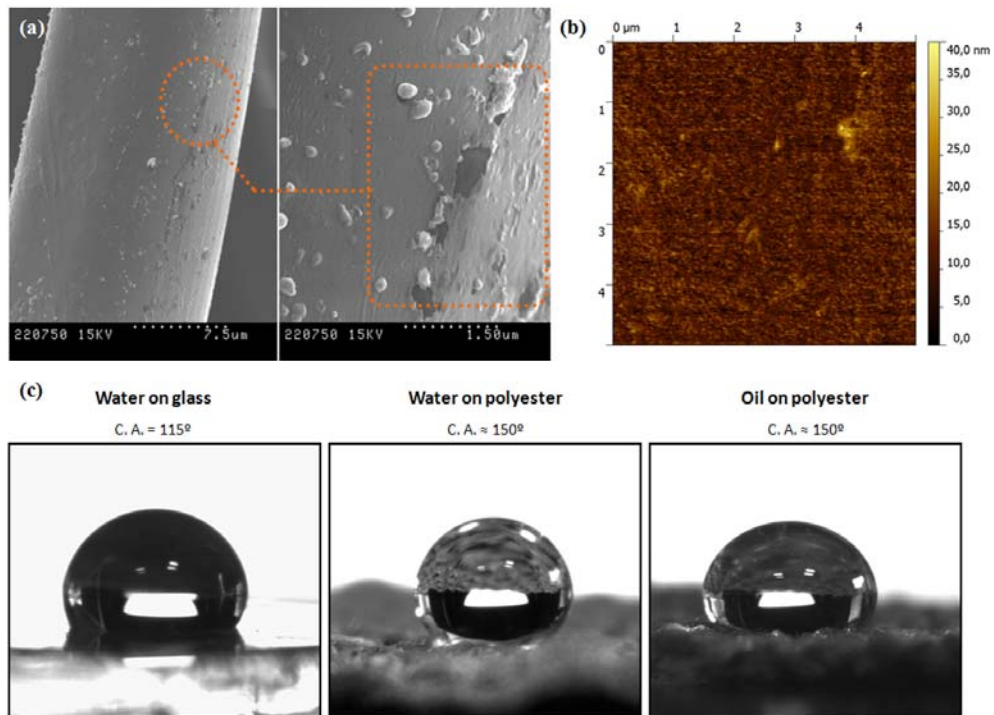


Figure 3

References

- [1] J.H. Waite, M.L. Tanzer, *Science* **1981**, *212*, 1038.
- [2] V. V. Papov, T. V. Diamond, K. Biemann, J. H. Waite, *J. Biol. Chem.* **1995**, *270*, 20183.
- [3] J.H. Waite, *Int. J. Adhesion and Adhesives* **1987**, *7*, 9.
- [4] T.J. Deming, *Curr. Opin. Chem. Biol.* **1999**, *3*, 100.
- [5] J.H. Waite, *Integr. Comp. Biol.* **2002**, *42*, 1172.
- [6] a) Q. Ye, F. Zhou, W. Liu, *Chem. Soc. Rev.* **2011**, *40*, 4244; b) H. Yamamoto, *Biotechnol. Genet. Eng.* **1995**, *13*, 133.
- [7] a) M. Yu, T. J. Deming, *Macromolecules* **1998**, *31*, 4739; b) B. P. Lee, C.-Y. Chao, F. N. Nunalee, E. Motan, K. R. Shull, P. B. Messersmith, *Macromolecules* **2006**, *39*, 1740; c) S. A. Burke, M. Ritter-Jones, B. P. Lee, P. B. Messersmith, *Biomed. Mater.* **2007**, *2*, 203.
- [8] a) S. Saxer, C. Portmann, S. Tosatti, K. Gademann, S. Zürcher, M. Textor, *Macromolecules* **2010**, *43*, 1050; b) H. Han, J. Wu, C. W. Avery, M. Mizutani, X. Jiang, M. Kamaigaito, Z. Chen, C. Xi, R. Lu, Y. Kamiya, T. Miyakoshi, *Talanta* **2006**, *70*, 370; c) B. Malisova, S. Tosatti, M. Textor, K. Gademann, S. Zürcher, *Langmuir* **2010**, *26*, 4018; d) J. L. Dalsin, L. Lin, S. Tosatti, J. Vörös, M. Textor, P. B. Messersmith, *Langmuir* **2005**, *21*, 640; e) J. L. Dalsin, B.-H. Hu, B. P. Lee, P. B. Messersmith, *J. Am. Chem. Soc.* **2003**, *125*, 4253.
- [9] H. Lee, S.M. Dellatore, W.M. Miller, P.B. Messersmith, *Science* **2007**, *318*, 426.
- [10] J. Sedó, J. Saiz-Poseu, F. Busqué, D. Ruiz-Molina, *Adv. Mat.* submitted.
- [11] H. Lee, J. Rho, P.B. Messersmith, *Adv. Mater.* **2009**, *21*, 431.
- [12] S. Kang, J. Rho, I.S. Choi, P.B. Messersmith, H. Lee, *J. Am. Chem. Soc.* **2009**, *131*, 13224.
- [13] a) J.H. Waite, *Nat. Mater.* **2008**, *7*, 8; b) C. Tao, S. Yang, J. Zhang, J. Wang, *Appl. Surf. Sci.* **2009**, *256*, 294; c) H.Y. Hu, B. Yu, Q. Ye, Y.S. Gu, F. Zhou, *Carbon* **2010**, *48*, 2347; d) S. Hong, K.Y. Kim, H.J. Wook, S.Y. Park, K.D. Lee, D.Y. Lee, H. Lee, *Nanomedicine* **2011**, *6*, 793; e) S.H. Ku, C.B. Park, *Biomaterials* **2010**, *31*, 9431; f) Y.M. Shin, H. Park, H. Shin, *Macromol. Res.* **2011**, *19*, 835; g) S.H. Yang, S.M. Kang, K.B. Lee, T.D. Chung, H. Lee, I.S. Choi, *J. Am. Chem. Soc.* **2011**, *133*, 2795.
- [14] J. Saiz-Poseu, J. Faraudo, A. Figueras, R. Alibés, F. Busqué, D. Ruiz-Molina, *Chem. Eur. J.* **2012**, *18*, 3056.
- [15] J. Kumanotani, *Prog. Org. Coat.* **1999**, *26*, 163.
- [16] A. A. R. Watt, J. P. Bothma, P. Meredith, *Soft Matter* **2009**, *5*, 3754

- [17] F. Bersmann, A. Ponche, C. Ringwald, J. Hemmerlé, J. Raya, B. Bechinger, J.-C. Voegel, P. Schaaf, V. Ball, *J. Phys. Chem. C* **2009**, *113*, 8234; b) D. R. Dreyer, D. J. Miller, B. D. Freeman, D. R. Paul, C. W. Bielawski, *Langmuir* **2012**, *28*, 6428.
- [18] a) X. Chao-Hua; Y. Wei; J. Shun-Tian *Nanotechnology* **2011**, *22*, 415603; b) A. Synytska, R. Khanum, L. Ionov, Ch. Cherif, C. Bellman *ACS Appl. Mater. Interfaces* **2011**, *3*, 1216; c) K. Nischala, T. N. Rao, N. Hebalkar *Colloids and Surfaces B-Bionterfaces* **2011**, *82*, 203.
- [19] a) W.-H. Zhou, C.-H. Lu, X.-C. Guo, F.-R. Chen, H.-H. Yang, X.-R. Wang, *J. Mater. Chem.* **2010**, *20*, 880-883; b) M. Zhang, X. He, L. Chen, Y. Zhang, *J. Mater. Chem.* **2010**, *20*, 10696-10704.
- [20] This thickness is very similar to that obtained for the polydopamine coatings previously reported: a) Penghua Yan, Jinqing Wang, Lin Wang, Bin Liu, Ziqiang Lei, Shengrong Yang, *Appl. Surf. Sci.* **2011**, *257*, 4849; b) B. Fei, B. Qian, Z. Yang, R. Wang, W. C. Liu, C. L. Mak, J. H. Xin, *Carbon* **2008**, *46*, 1792.
- [21] a) K.-H. Cho, L. -J. Chen, *Nanotechnology* **2011**, *22*, 445706; b) T. Nishin, M. Meguro, K. Nakamae, M. Matsushita, Y. Ueda, *Langmuir* **1999**, *15*, 4321.
- [22] a) M.H. Ryou, Y.M. Lee, J.K. Park, J.W. Choi, *Adv. Mater.* **2011**, *23*, 3066. b) B. Yu, J.X. Liu, S.J. Liu, F. Zhou, *Chem. Commun.* **2010**, *46*, 5900. c) S.M. Kang, I. You, W.K. Cho, H.K. Shon, T.G. Lee, I.S. Choi, J.M. Karp, H. Lee, *Angew. Chem., Int. Ed.* **2010**, *49*, 9401.
- [23] X.-L. Zheng, J.-B. Weng, Q.-M. Huang, B.-H. Hu, T. Qiao, P. Deng, *Colloid Surf. A* **2009**, *337*, 15.

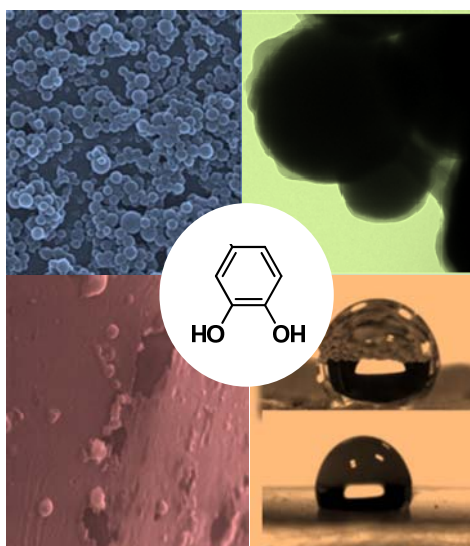
Table of contents entry

A facile one-step polymerization strategy is explored to achieve uniform catechol-based materials. Depending on the functionality of the catechol, the as-prepared product can be used as a coating to systematically modify the surface tension from oleo-/hydrophobic to highly hydrophilic materials, both on nano and bulk structures, as well as to self-assemble as solid nanoparticles with sticky properties in polar solvent media. Such a versatile concept is ideal for the development of catechol-based multifunctional materials.

Keyword: catechol, adhesive properties, coatings, oleo-/hydrophobic-hydrophilic, nanoparticles

J. Saiz-Poseu, J. Sedó, B. García, C. Beneiges, R. Alibés J. Hernando, F. Busqué and D. Ruiz-Molina*

Versatile Functional Materials via Direct Polymerization of Catechols



Supplementary material for:

*Versatile Functional Materials via Direct Polymerization of
Catechols*

by Saiz-Poseu et al.

S1. Synthesis and characterization of compounds 1-3



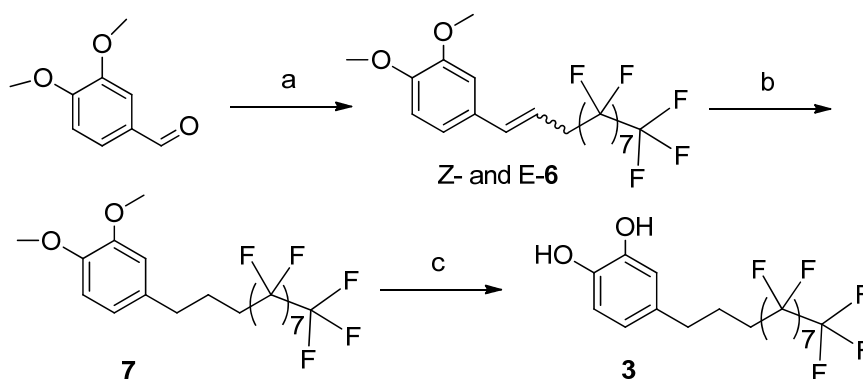
Catechol **1** was synthesized as previously described.¹ Catechol **4** was obtained from Sigma-Aldrich. Commercially available reagents were used as received. Solvents were dried by distillation over appropriate drying agents. All reactions were performed avoiding moisture by standard procedures and under nitrogen atmosphere, and were monitored by analytical thin layer chromatography (TLC) using silica gel F254 pre-coated aluminium plates (0.25 mm thickness). Flash column

chromatography was carried out using silica gel 60 (particle size 35-70).

Chemical characterization. ¹H-NMR spectra were recorded on a Bruker DPX250 spectrometer (250 MHz, CDCl₃, δ = 7.26 ppm). ¹³C-NMR spectra were recorded on a Bruker DPX250 spectrometer (62.5 MHz; CDCl₃, δ = 77.2 ppm /Acetone-d₆, δ = 39.5 ppm), with complete proton decoupling. Infrared spectra were recorded on a Sapphire-ATR Spectrophotometer. High resolution mass spectra (HRMS) were recorded with a Micromass-AutoSpec using (ESI+). X-ray photoelectron spectroscopy (XPS) analyses were conducted in order to identify the chemical states of the elements with a PHI 5550 Multisystem spectrometer with a monochromatic Al Kα radiation (1486.6 eV). Direct current (dc) magnetic susceptibility measurements were carried out on a Quantum Design MPMS SQUID susceptometer with a 55 kG magnet and operating in the range of 1.7e320 K. All measurements were collected in a field of 10 kG. Background correction data were collected from magnetic susceptibility measurements on the holder capsules. Diamagnetic corrections estimated from the Pascal contents were applied to all data for determination of the molar paramagnetic susceptibilities of the compounds.

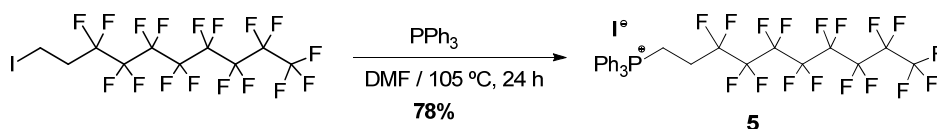
EPR spectra were recorded on a Bruker ESP-300E spectrometer operating in the X-band (9.3 GHz). Signal-to-noise ratio was increased by accumulation of scans using the F/F lock accessory to guarantee a high-field reproducibility. Precautions to avoid undesirable spectral line broadening such as that arising from microwave power saturation and magnetic field over modulation were taken. To avoid dipolar broadening, the solutions were carefully degassed three times using vacuum cycles with pure argon. The g-value was determined against the DPPH standard ($g \approx 2.0023$).

S1.1. Synthetic route for catechol 3



Synthetic route for catechol **3**. a) $[\text{Ph}_3\text{PCH}_2\text{CH}_2\text{RF}_8]^+\text{I}^-$, K_2CO_3 , dioxane, 95°C , 77%; b) H_2 , Pd/C 10%, EtOAc, rt, 95%; c) BBr_3 , CH_2Cl_2 , -5°C , 90%.

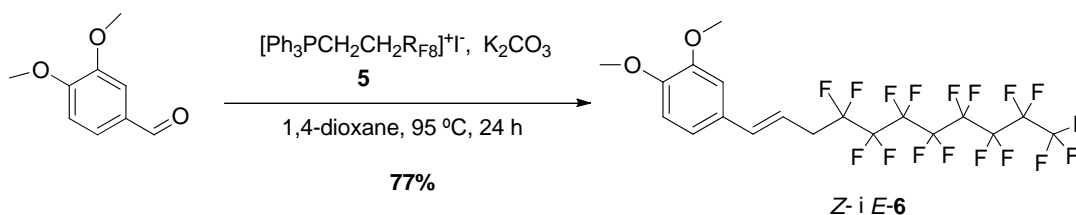
(3,3,4,4,5,5,6,6,7,7,8,8,9,9,10,10,10heptafluorodecyl) triphenylphosphonium iodide, **5**



A mixture of 10.27 g of 1-iodo-1*H*,1*H*,2*H*,2*H*-perfluorodecane and 5.16 g of triphenylphosphine in 10 ml of dry DMF is heated to 105°C for 24 hours. After cooling to room temperature, CH_2Cl_2 (60 ml) and water (30 mL) were added to the reaction

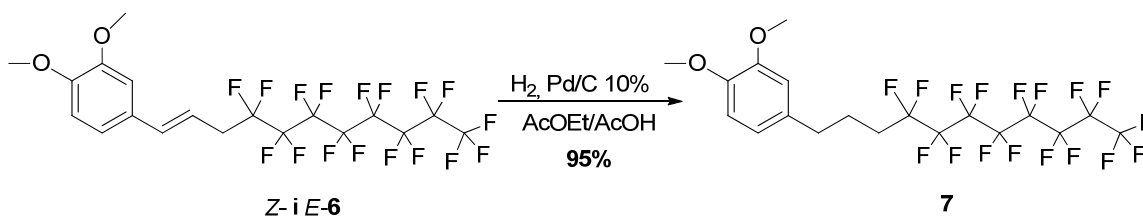
mixture, the phases were separated and the aqueous was extracted with methylene chloride (3x30 mL). The combined organic phases were dried over MgSO₄ and concentrated under vacuum, affording a yellow solid which is washed with ethyl ether (2x20 mL) yielding pure **5** as a white solid (11.65 g, 78% yield).

(Z)- and (E)-4-(4,4,5,5,6,6,7,7,8,8,9,9,10,10,11,11-hexadecafluorododec-1-enyl)-1,2-dimethoxybenzene (6).



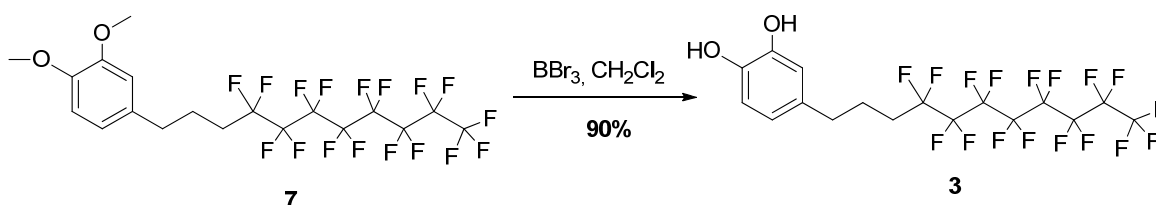
A mixture of (4,4,5,5,6,6,7,7,8,8,9,9,10,10,11,11-hexadecafluorododecyl)-triphenylphosphonium iodide (5.52 g, 6.61 mmol), K₂CO₃ (2.56 g, 18.52 mmol) and 3,4-dimethoxybenzaldehyde (1.0 g, 6.02 mmol) was suspended in dioxane (25 mL) and heated to 75 °C for 24 hours. After cooling to room temperature water (30 mL) was added, the phases were separated and the aqueous was extracted with methylene chloride (3x30 mL). The combined organic phases were dried over MgSO₄ and concentrated under vacuum, affording an oil that was purified by column chromatography on silica gel with hexanes/EtOAc (4:1) to give a (≈ 10:1) mixture of (Z)- and (E)-**6** as a solid (3.59 g, 78% yield). A second column chromatography easily allowed the isolation of pure major isomer (Z)-**9**. (Z)-**9**: ¹H NMR (250 MHz, CDCl₃, δ): 6.90-6.73 (m, 4H), 5.66 (dt, *J* = 11.0, 7.1 Hz, 1H), 3.89 (s, 3H), 3.87 (s, 3H), 3.12 (td, *J* = 18.2, 7.1 Hz, 2H); ¹³C NMR (62.5 MHz, CDCl₃, δ): 149.3, 149.0, 135.7, 129.1, 121.4, 117.1, 112.1, 111.5, 56.2, 56.1, 31.0 (t, *J*_{CF} = 22 Hz); IR (ATR, ν): 2962, 1517, 1198, 1145, 1023 cm⁻¹; Mp: 35-37 °C; HRMS (ESI+, *m/z*): [M+Na]⁺ calcd. for C₁₉H₁₃F₁₇O₂Na 619.0536; found: 619.0544.

4-(4,4,5,5,6,6,7,7,8,8,9,9,10,10,11,11-hexadecafluorododecyl)-1,2-dimethoxybenzene (7).



A stirred solution of a mixture of (*Z*)- and (*E*)-**6** (1.0 g, 1.68 mmol) in EtOAc (20 mL) was hydrogenated over Pd/C (31 mg) under 1 atm of H₂ for 24 h. The catalyst was removed by filtration over Celite and the solvent was evaporated to afford **7** as a colorless solid (0.97 g, 98% yield). ¹H NMR (250 MHz, CDCl₃, δ): 6.82-6.70 (m, 3H), 3.87 (s, 3H), 3.86 (s, 3H), 2.65 (t, *J* = 7.3 Hz, 2H), 2.18-1.89 (m, 4H); ¹³C NMR (62.5 MHz, CDCl₃, δ): 149.3, 147.8, 133.4, 120.4, 111.8, 111.6, 56.1, 56.0, 34.8, 30.4 (t, *J*_{CF} = 2.2 Hz), 22.2 (t, *J*_{CF} = 3 Hz); IR (ATR, ν): 2924, 1518, 1197, 1143, 1023 cm⁻¹; Mp: 64-66 °C; HRMS (ESI+, *m/z*): [M+Na]⁺ calcd. for C₁₉H₁₅F₁₇O₂Na 621.0693; found: 621.0698.

4-(4,4,5,5,6,6,7,7,8,8,9,9,10,10,11,11-hexadecafluorododecyl)catechol (3).



Compound **7** (0.59 g, 0.98 mmol) was dissolved in CH₂Cl₂ (4 mL) under nitrogen atmosphere. The mixture was cooled down to -5 °C and BBr₃ (7.9 mL, 7.90 mmol) was added dropwise. After stirring for 1 h, the reaction was allowed to warm up to 0 °C and then quenched with water (20 mL), the phases were separated and the aqueous was extracted with methylene chloride (3 x 30 mL). The combined organic phases were dried over MgSO₄ and concentrated under vacuum, affording an oil that was purified by column chromatography on silica gel with hexanes/EtOAc (4:1) to provide **3** (0.52 g, 90% yield) as a white solid. ¹H NMR (250 MHz, CDCl₃, δ): 7.72 (broad s, 2H), 6.77 (d, *J* = 8.0 Hz, 1H), 6.75 (d, *J* = 2.1 Hz, 1H), 6.58 (dd, *J* = 8.0, 2.1 Hz, 1H), 2.63 (t, *J* =

7.3 Hz, 2H), 2.30-2.15 (m, 2H), 1.93-1.85 (m, 2H); ^{13}C NMR (62.5 MHz, CDCl_3 , δ): 145.1, 143.4, 132.5, 119.6, 115.4, 115.2, 33.8, 29.8 (t, $J_{\text{CF}} = 22.3$ Hz), 22.0 (t, $J_{\text{CF}} = 3.0$ Hz); IR (ATR, ν): 3268, 2924, 1230, 1197, 1144, 1023 cm^{-1} ; Mp: 111-114 $^{\circ}\text{C}$; HRMS (ESI+, m/z): $[\text{M}+\text{Na}]^+$ calcd. for $\text{C}_{17}\text{H}_{11}\text{F}_{17}\text{O}_2\text{Na}$ 569.0415; found: 569.0431.

S1.2. Synthesis and characterization of **2**

Catechol **1** (0.5 g) were dissolved in methanol (250 ml, 0.2% w/v) at 40 $^{\circ}\text{C}$. Then, a 100 molar excess of ammonia (25% aqueous solution) was added drop wise under magnetic stirring. After 24 hours 115 ml of water were added and the excess of ammonia and the methanol were removed by evaporation under reduced pressure. The mixture was treated with drops of concentrated HCl until the pH was slightly acidic (≈ 5) and then the product was extracted with chloroform and dried over MgSO_4 and concentrated under reduced pressure yielding **1p** (495 mg) as a dark brown solid.

FT-IR. Peaks corresponding to the aliphatic chain (that can also be observed in the IR spectrum of **1**) are clearly seen at 2918 cm^{-1} , 2850 cm^{-1} (C-H st), 1466 cm^{-1} (C-H bend) and at 720 cm^{-1} ($-(\text{CH}_2)_n-$ rocking in long alkyl chains). In addition, three new broad and smaller peaks (not present in the starting material) show up at 1676 cm^{-1} , 1572 cm^{-1} and 1504 cm^{-1} . The peak at 1676 cm^{-1} may correspond to the presence of conjugated carbonyl groups in *o*-quinone moieties, arising from the oxidation of catechol rings. Nevertheless, this peak, together with that observed at 1572 cm^{-1} , could also be assigned to the C=N st band of imines.

NMR, ESR & SQUID Magnetization analysis. ^1H - and ^{13}C -NMR of **2** in CDCl_3 are shown in **Fig. S1**. Both exhibit signals corresponding exclusively to part of the aliphatic protons of the heptadecyl chain. The lack of signals arising from aromatic protons was initially attributed to a complete substitution of these through subsequent steps of oxidation and Michael-type nucleophilic attack by ammonia. However, the fact that

aromatic carbons are not observed either in the ^{13}C -NMR spectrum –where, once more, only signals corresponding to part of aliphatic nuclei can be observed- suggests that the underlying cause is probably more complex.

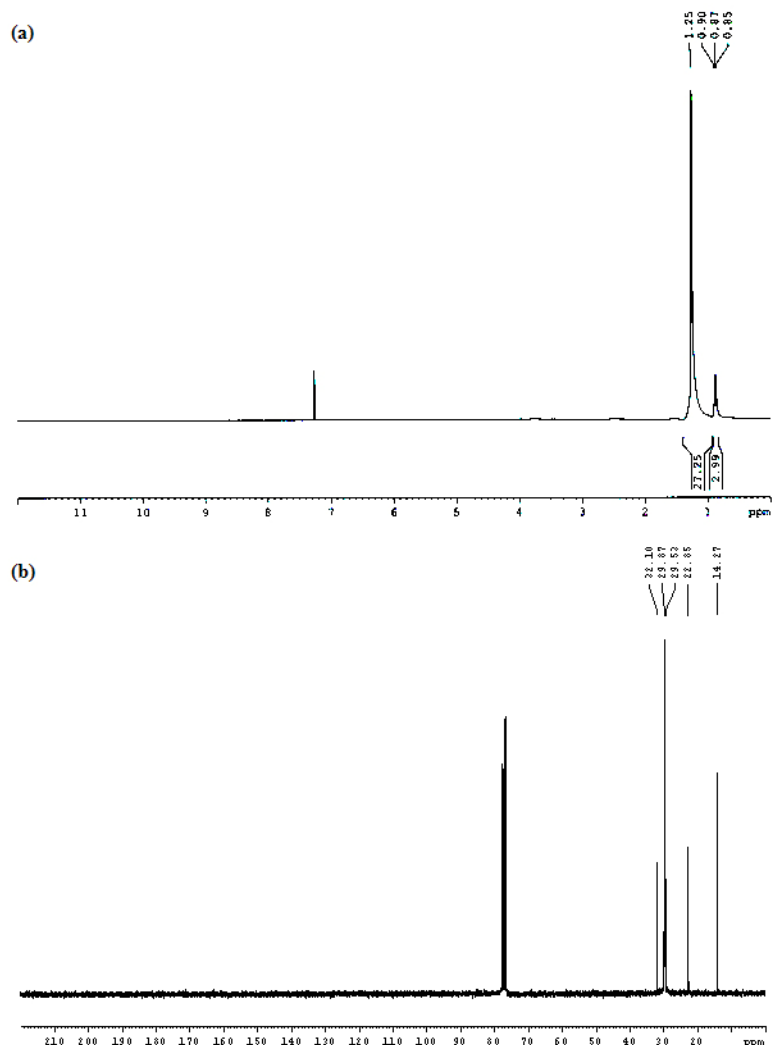


Figure S.1. NMR characterization of **2**. (a) ^1H -NMR (CDCl₃) spectrum and (b) ^{13}C -NMR spectrum (CDCl₃).

Another possible explanation for the above-mentioned anomalies in NMR spectra would be the presence of free radicals in the aromatic moieties, inducing paramagnetic shifts resulting in the displacement, broadening and eventual disappearance of certain signals. Since catechols are well-known to coexist in different oxidation states, it would not be surprising to find a sizeable fraction of aromatic rings in a radical, semiquinone

state. To fully assess or discard this possibility, electron paramagnetic resonance (EPR) experiments were carried out, showing ill-defined and low-level signals, attributable to radical impurities with a g value close to that expected for an organic radical ($g \approx 2.0023$). This hypothesis was confirmed by SQUID magnetization measurements (5-300 K temperature range) on solid samples, which confirmed that polymer **2** is essentially diamagnetic, with paramagnetic impurities accounting for less than 1% of the sample weight according with the resulting magnetization moment at room temperature ($C=0.0025 \text{ emu.K.mol}^{-1}$). In conclusion, the lack of ^1H and ^{13}C -NMR signals from nuclei making up the aromatic ring and part of the aliphatic chain were attributed to a bad relaxation of their magnetization.

Mass spectrometry. The sample was dissolved in hexane in a concentration of 1 mg/ml and diluted in ethanol (1:10 v/v). The resulting mixture was injected in the mass spectrometer. The distribution of masses obtained through ESI (+) with a declustering potential of 50 V (used to avoid possible aggregation effects in the measurement) shows several main signals, among them two important signals at 685 and 1745 (m/z), which would be coincident with structures closely related to a dimer and a pentamer of **1** respectively. At 1448 and 2411 (m/z), two minor signals can also be appreciated, whose masses would be related with a tetramer and a heptamer of **1** respectively. Moreover, when experiments were done at higher decoupling voltages (100, 150 and 200 V), similar results were obtained. This would indicate that monomer structures are linked through covalent bonds, rather than supramolecular interactions such as hydrogen bonds or π - π stacking, giving rise to oligomeric species with no more than 6-7 catecholic and/or catechol-derived units.

Elemental analysis. Elemental analysis of a sample of **2** purified by flash column chromatography showed the presence of nitrogen (C: 65.47%; H: 10.03%; N : 3.19%).

This percentage is consistent with the incorporation of roughly one nitrogen atom per catechol unit, although there is still a significant percentage of the sample mass that remains unaccounted for, which could be attributed to oxygen, most likely coming from residual solvents.

XPS experiments. The XPS spectra of an aluminum substrate, both coated and untreated are shown in **Fig. S2**.

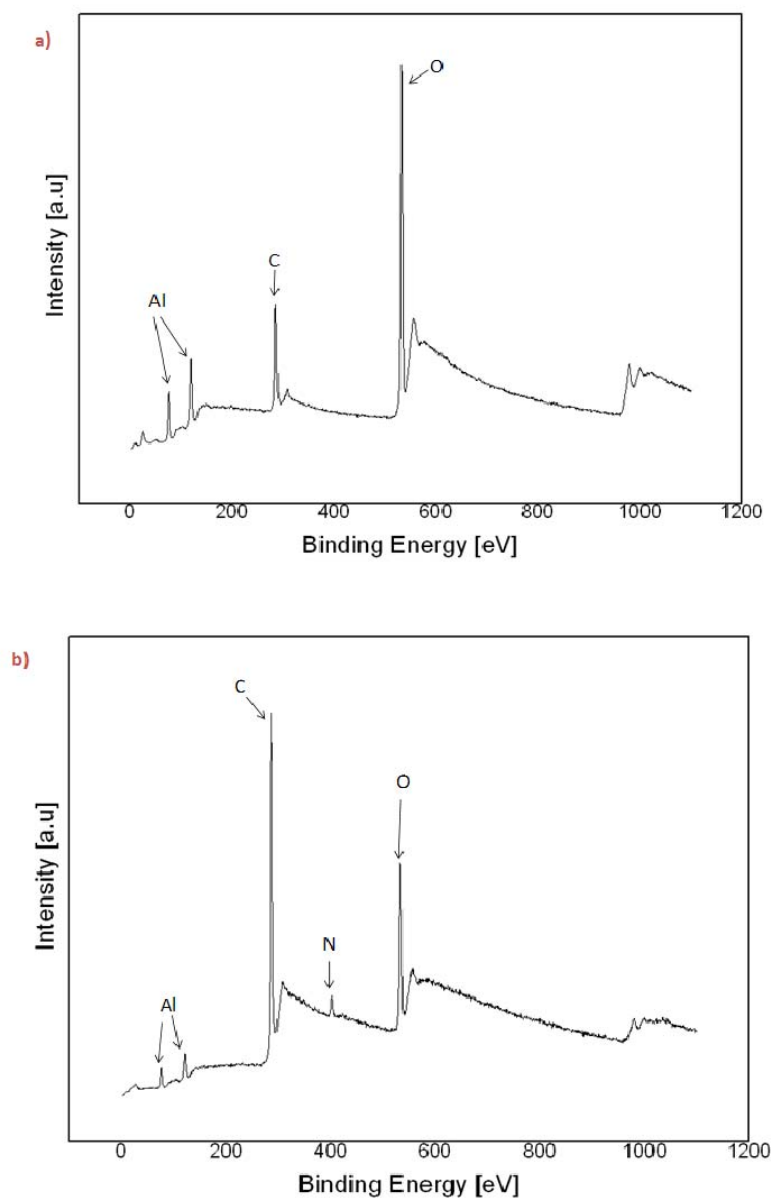


Figure S2. XPS spectra of (a) blank aluminium substrate and (b) coated substrate with 2.

The initial XPS spectrum of an uncoated aluminum substrate reveals an emission peak coming from the carbon due to the presence of environmental impurities.

Simultaneously peaks associated to the aluminum (substrate) and oxygen (coming from surface oxides and aluminum hydroxides) can clearly be differentiated. In the XPS spectrum of the coated substrate, in addition to the peaks previously described, a new peak associated to the presence of the nitrogen can be clearly distinguished, confirming the addition of ammonia to the catechol. Simultaneously, an increase of the peak ratio C/Al is observed while the intensity of the signals associated to oxygen and aluminum decrease. This is coherent with the presence of an organic coating mostly of carbonated nature, supported by the slight color change observed upon exposition.

S2. Physical characterization techniques

Contact Angle (CA). The CA of miliQ water droplets (3 μ L) on coated substrates was used to evaluate the hydrophobicity of all coatings at room temperature by means of the “sessile drop” technique. An Easy Drop Standard analyzer and the Drop Shape Analysis DSA 10 software (Krüss, Hamburg) were used throughout. The reported values arise from averaging CA measurements on five different zones of each sample.

Optical Microscopy. Optical microscopy images were obtained with an Axio Observer Z-1m (Zeiss) inverted optical microscope, equipped with five different magnification lenses (5x, 10x, 20x, 50x and 100x), and an XY motorized sample holder. The excitation source used was a short-arc high pressure Hg lamp (HBO 103/2, 100W).

Atomic Force Microscopy. AFM images were obtained at room temperature with an AFM/SPM Agilent 5500 microscope, acoustically isolated and placed on a granite base. NCHR PointProbe-Plus silicon nitride tips (Nanosensors Inc.; force constant \approx 42 N/m,

resonance frequency ≈ 270 KHz) were used, with the equipment operating in tapping mode. Images were treated with WSxM 5.0 free software (Nanotec Electronica SL).

Scanning Electron Microscopy. SEM measurements were carried out with a HITACHI S-570 and a QUANTA FEI 200 FEG-ESEM, both operating at 15 kV. Samples for the observation of nanoparticles were prepared by casting a drop of the corresponding dispersion on aluminium tape, and further evaporation of the solvent at room temperature. In the case of macroscopic objects (polyester fibers and glass), coated substrates were fixed on SEM holders using adhesive carbon tape. Prior to observation with SEM, all samples were metalized with a thin layer of gold using a sputter coater K550 (Emitech).

Transmission Electron Microscopy. TEM images were obtained with a high-resolution Jeol JEM-2011 microscope operating at 200 kV and a Jeol JEM-1400 microscope operating at 120 kV. In both cases, samples were prepared by casting a drop of the corresponding nano-object dispersion on a holey carbon copper grid, and further evaporating the solvent at room temperature. The Jeol JEM-2011 apparatus was also used for determining the presence of metal species by EDS and for detecting the presence of crystalline structures by X-ray diffraction. In order to preserve the structure of the nanoparticles in the dispersions, some samples were observed in a cryogenic state, freezing the drop by means of a Leica EM-CPC controlled environment vitrification system.

S3. Nanoparticle coating

Iron oxide nanoparticles of 500-650 nm in diameter were dispersed in a 0.5% (w/v) *n*-hexane solution of **2** for 30 minutes and filtered. TEM images shown in **Fig. S3** reveal

that treated NPs appear surrounded by a brighter halo (not apparent in the non-treated sample) that corresponds to the presence of a 5 to 50 nm thin film of **2**.^[2]

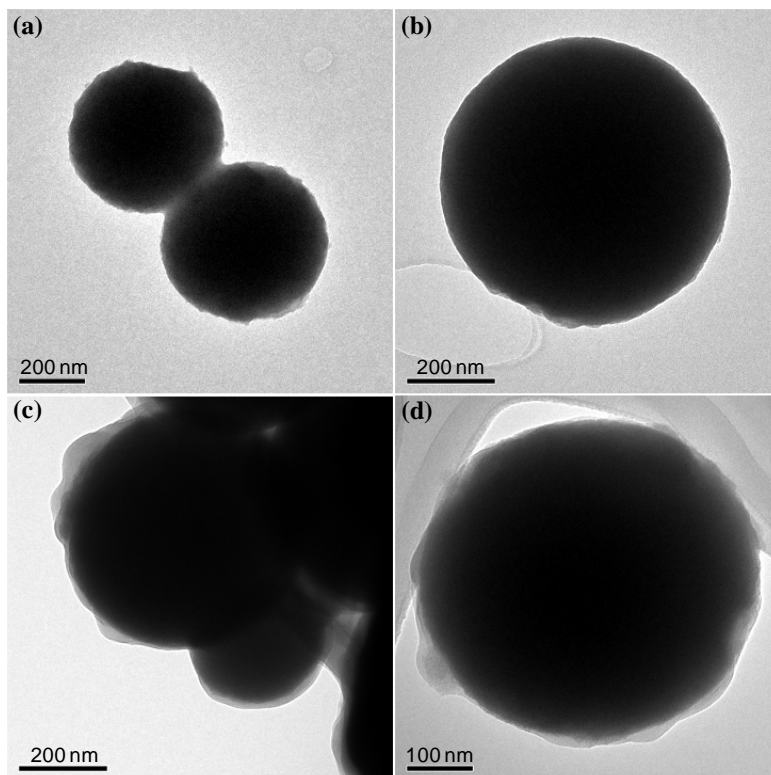


Figure S3. TEM images of iron oxide nanoparticles. (a) and (b) Blank NPs. (c) and (d) treated NPs with a 0.5% w/v *n*-hexane solution of **2** for 30 minutes, from where the coating can be appreciated as a lighter envelope.

Similar results were obtained for 250-600 nm mesoporous silica NPs, affording coating thicknesses ranging from 7 to 20 nm (see **Fig. S4**).

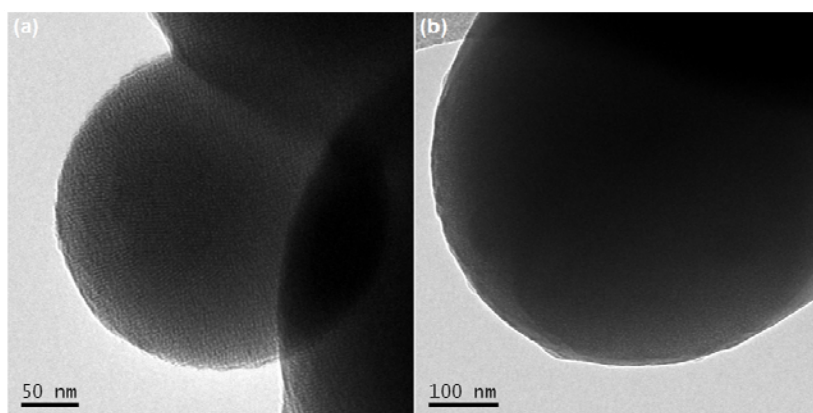


Figure S4. TEM images of mesoporous silica nanoparticles (a) Blank NPs and (b) NPs treated with a 0.5 % (w/v) *n*-hexane solution of **2** for 30 minutes, from where the coating can be appreciated as a lighter envelope.

S4. Glass coating

S4.1. Coating with **1**

The capacity to coat a glass slide with a self-assembly (SAM) monolayer of catechol **1** in acetonitrile (1%, w/v) for different immersion times was studied for comparison purposes. The results are shown in **Fig. S5**.

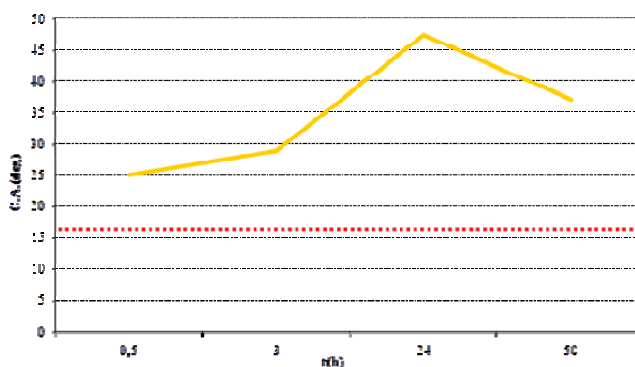


Figure S5. Contact angle (CA) of a glass substrate immersed for different times in an acetonitrile solution of **1** (1%, w/v). The red dashed line indicates the contact angle value obtained with a non-treated glass.

As can be seen there, right after 30 minutes there is an increase of the CA value from 15° for the non-treated sample to approximately 25°. This value continues increasing up to a maximum of 47° after 24 hours. A feasible explanation for this increase can be tentatively associated to the formation of a SAM considering the literature precedents reporting catechols interaction with differently silicates³ and the presence of the alkyl chains that can give the hydrophobic character. However, the CA values achieved are considerable smaller than those obtained for **2**, as well as the resistance of the coating, which fails to maintain the droplet for long times.

Finally, a drop of the CA value is observed for immersion times longer than 24 hours.

The reason is that the surface gets coated with structures a few nanometers size that

most likely correspond to molecular aggregates, as confirmed by AFM experiments (see **Fig. S6**).

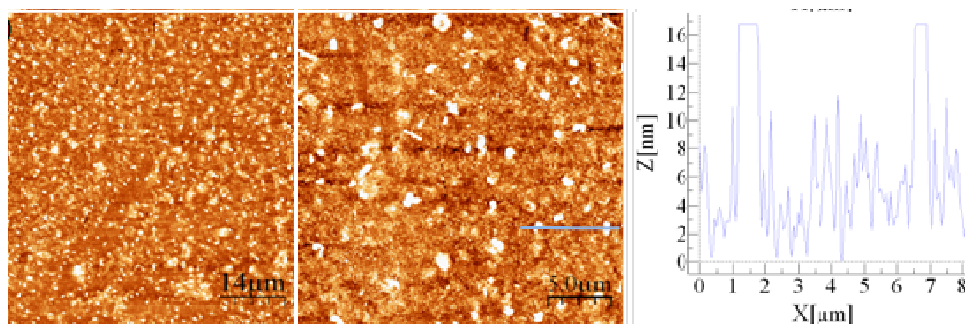


Figure S6. AFM images of glass substrates treated with an acetonitrile solution of **1** (1%, w/v) for 50 hours.

S4.2. Coating with **2**

A glass slide was brought in contact with a 1% (w/v) *n*-hexane solution of **2** for 1 minute. To rule out the existence of an excessive adsorption contributing to the measured thickness, the sample was rinsed twice with methanol before proceeding to the AFM measurements. Relevant information about the morphology of the resulting coating layer can be extracted from the corresponding images shown in **Fig. S7**. The resulting coating is very homogeneous with a surface roughness inferior to 0.2 nm. The width of the homogenous layer was studied by manually generating a scratch with a hypodermic needle, resulting to be of approximately 150 nm. This thickness cannot be associated to the presence of simple molecular layers, being most likely formed by a multi-layered material deposition.

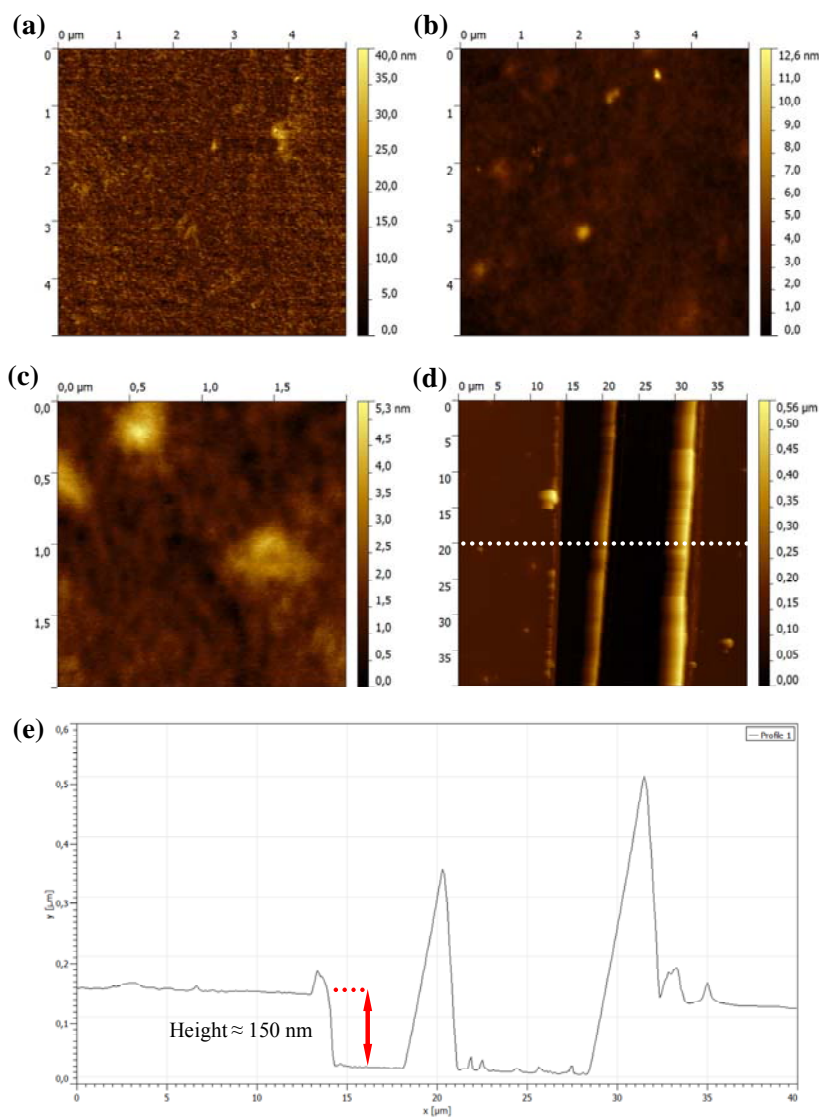


Figure S7. AFM topography images of a 5 μm x 5 μm glass substrate: (a) blank glass exhibiting an average roughness of 2.2 nm. (b) The same piece of glass upon coating with a 1% (w/v) *n*-hexane solution of **2** for 1 minute exhibiting an average roughness of 0.2 nm. (c) AFM amplification of a 2 μm x 2 μm area. (d) Wide view (40 μm x 40 μm) of a manually scratched zone. (e) Profile marked as a white dashed line in (d), where the coating height is measured as the depth of the scratch.

S4.3. Coating optimization of **2**

Glass slides were used as models to establish the influence of two main parameters (solvent nature and concentration) on the hydrophobic effectiveness of the coating. No significant variations were observed at different immersion times ranging from 1 minute to 24 hours.

Solvent. A glass slide is brought in contact with a 1% (w/v) solution of **2** for 1 minute in four different solvents, always avoiding the use of polar solvents that have been shown to favour the aggregation of the material as nanoparticles. The results are shown in **Fig. S8**.

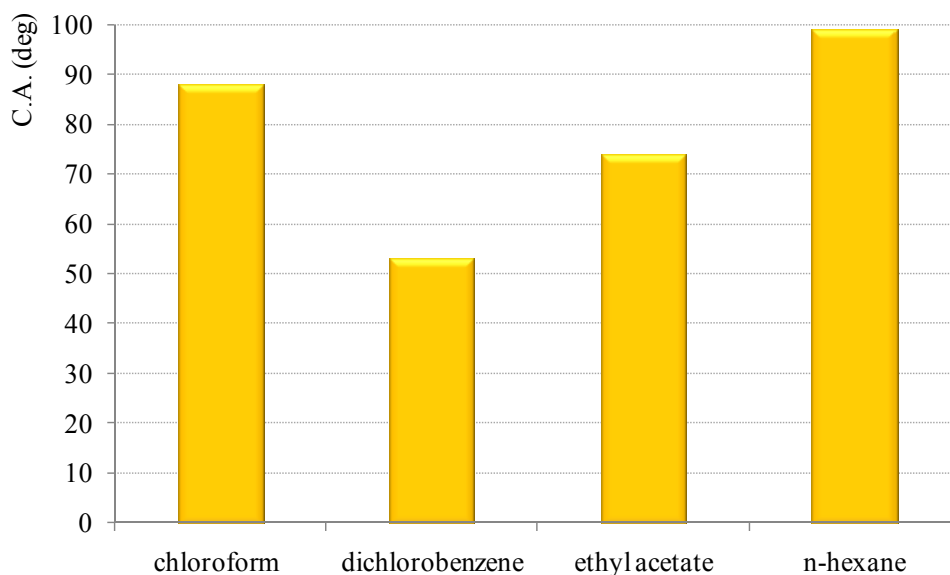


Figure S8. Contact angle for a glass substrate treated with a 1% (w/v) solution of **2** for 1 minute in different solvents.

Best results were obtained with chloroform and hexane, where contact angles between 90° and 100° are achieved. Worse results are obtained when using ethyl acetate and especially dichlorobenzene as a solvent, giving rise to contact angles that can go down to 50°. In any case, this value is considerable larger than that obtained for the rough untreated glass that oscillates between 15-20°.

According with the results previously described, hexane was the solvent of choice to do all the coating experiments along the present project.

Concentration effect. The concentration effect of **2** on the hydrophobic coating was studied in hexane at two four different concentrations (0.1, 1.0, 5.0 and 10.0%). The results are shown in **Fig. S9**. Overall, an increase of the CA values with the concentration is observed up to 1%. From there, the value is more or less maintained.

Considering these results, and to save a 5 fold amount of material, 1% is considered as a good balance between hydrophobicity and economy of the process.

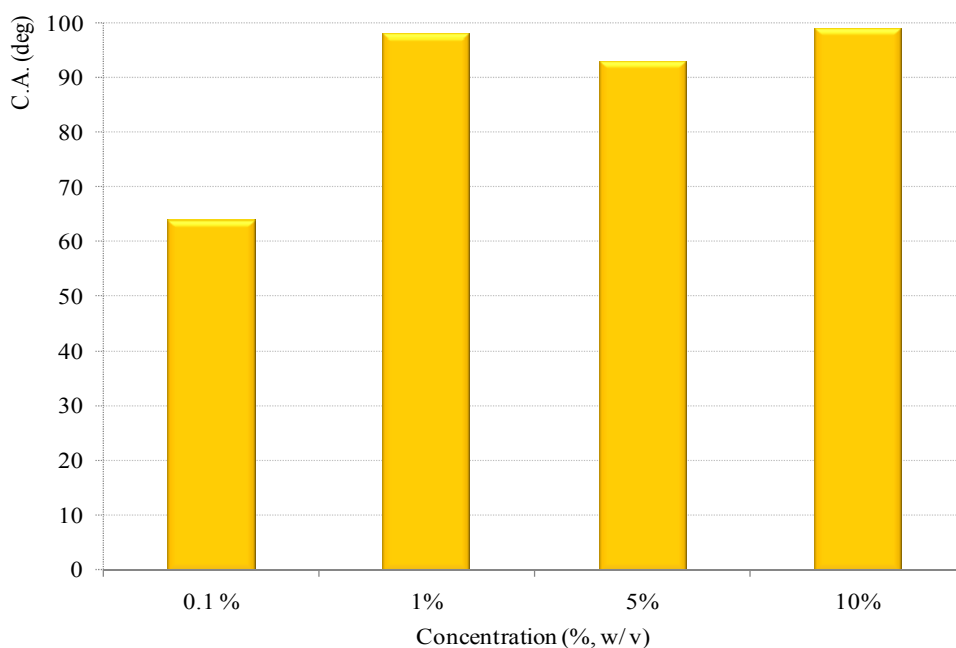


Figure S9. Contact angle values for glass substrates treated with a *n*-hexane solution of **2** at four different concentrations for 1 minute.

S5. Polyester coating with a *n*-hexane solutions of **2**

In a typical experiment a 2 x 2 cm polyester piece is brought in contact with a *n*-hexane solution of **2** at different concentrations. Afterwards, the piece is removed from the solution, dried and the resulting surface studied by SEM and contact angle measurements. An increase of the concentration from 1% to 10% (w/v) leads to an increase of the amount of the material that coats the fibers, as can be seen in **Fig. S10**. Nevertheless, it can also be observed that the treatment only affects the fibers. The coating is not occupying the voids between them, not even for this higher concentration. This fact is very important since, in this way, the mechanical properties and transpirability of the textiles are preserved. Important to emphasize, there is not a

significant modification of the resulting contact angles along the range of concentrations used, which oscillate in all the cases around 140°.

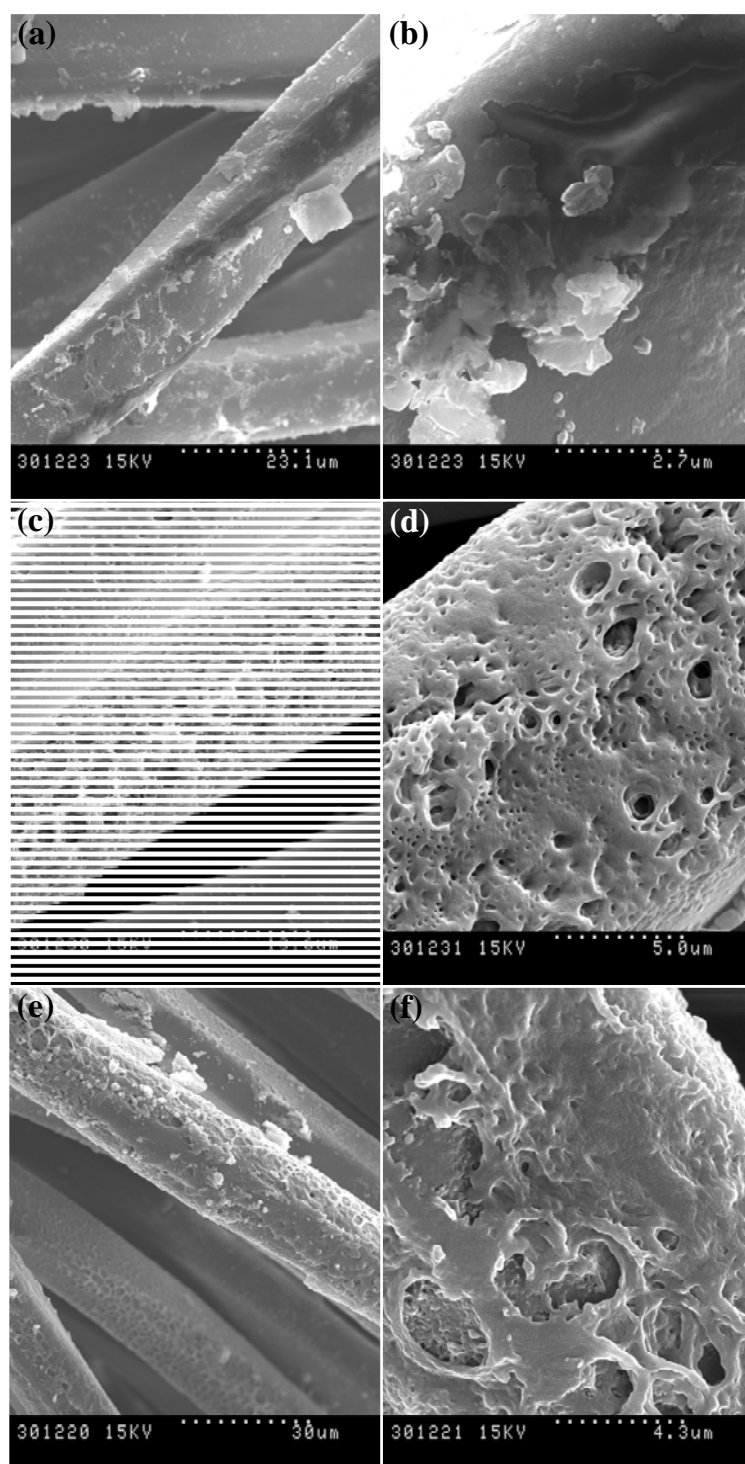


Figure S10. SEM images of polyester fibers treated with *n*-hexane solutions of **2** at different concentration for 1 minute. (a) and (b) [**2**] = 1% (w/v). (c) and (d) [**2**] = 5% (w/v). (e) and (f) [**2**] = 10% (w/v).

[1] J. Saiz-Poseu, J. Faraudo, A. Figueras, R. Alibes, F. Busqué, D. Ruiz-Molina, *Chem. Eur. J.* **2012**, *18*, 3056.

[2] a) W.-H. Zhou, C.-H. Lu, X.-C. Guo, F.-R. Chen, H.-H. Yang, X.-R. Wang, *J. Mater. Chem.* **2010**, *20*, 880-883; b) M. Zhang, X. He, L. Chen, Y. Zhang, *J. Mater. Chem.* **2010**, *20*, 10696-10704.

[3] a) H. Han, J. Wu, C. W. Avery, M. Mizutani, X. Jiang, M. Kamigaito, Z. Chen, C. Xi, K. Kuroda, *Langmuir* **2011**, *27*, 4010-4019; b) T. H. Anderson, J. Yu, A. Estrada, M. U. Hammer, J. H. Waite, J. N. Israelachvili, *Adv. Funct. Mater.* **2010**, *20*, 4196-4205.